Imaging of one- and two-dimensional Fiske modes in Josephson tunnel junctions

B. Mayer, T. Doderer, and R. P. Huebener
Physikalisches Institut, Lehrstuhl Experimentalphysik II, Universität Tübingen, W-7400 Tübingen, Federal Republic of Germany

A. V. Ustinov
Institute of Solid State Physics, U.S.S.R. Academy of Sciences, Chernogolovka, Moscow District, 142432, U.S.S.R.
(Received 17 June 1991)

We report on spatially resolved measurements of dynamic states of Josephson tunnel junctions in an external magnetic field. Using low-temperature scanning electron microscopy we imaged the beam-induced change of the maximum Fiske-step currents and the voltage change of current-biased step states. The excitation of one- and two-dimensional self-resonant cavity modes is clearly visible with a spatial resolution of about 3 μm. We used a 50×50 μm^2 $Nb/Al_2O_3/Nb$ tunnel junction representing a junction of intermediate size. Our experimental results agree well with a qualitative model for the signal generation based on the global change of the junction quality factor Q due to the local electron-beam irradiation. In addition, we present results of a calculation based on the perturbed sine-Gordon equation that takes into account the suppression of the critical current density in the area of the electron beam irradiation.

I. INTRODUCTION

Recently, low-temperature scanning electron microscopy (LTSEM) as a combination of a standard SEM equipment and a liquid-He-cooled cryostage has been used to investigate various low-temperature phenomena[1] such as superconductivity, ballistic phonon propagation,[2,3] or dissipative structures in semiconductors.[4,5] Especially for superconducting thin films and Josephson tunnel junctions LTSEM is a powerful tool to obtain two-dimensional images showing different physical properties of the samples.[6] Another important application of LTSEM is the *characterization* of high-T_C superconducting thin films at the microscopic level. Here, it is possible to obtain information about the spatial homogeneity of the critical current density and the resistive transition.[7,8]

In the last years two different measuring techniques (voltage image, current image) were developed to get a deeper insight into the behavior of Josephson junctions. For the voltage image the junction is current biased while the electron beam is scanned across the junction area and the beam-induced voltage change ΔV of the whole junction due to the local irradiation is detected. Using the voltage imaging technique, LTSEM shows the spatial distribution of the quasiparticle current density[9] as well as that of the energy gap.[10] The current imaging method uses, for example, the beam-induced change of the maximum zero-voltage current $\Delta I^{\max}$ as a function of the beam position (x_0,y_0) on the junction surface. With this technique it is possible to image the spatial distribution of the Josephson pair-current density,[11–13] static Josephson vortices or trapped magnetic flux quanta.[14,15] The spatially resolved measurements contain detailed information not provided by the current-voltage-characteristic (IVC) measurements alone where only time- and space-integrated current and voltage signals are obtained.

Experimental data on spatially resolved measurements of dynamic modes in Josephson tunnel junctions have been given by Meepagala *et al.*[16,17] They used a laser scanning technique to investigate the zero-field current steps at finite voltages in one-dimensional junctions. However, their spatial resolution is limited by the diameter of the focused laser beam which is typically in the range of 40 μm. Therefore the resolution is at least 1 order of magnitude lower than for LTSEM.

In this paper we report on the application of the two LTSEM measuring techniques described above to the well-known Fiske steps.[18,19] In the presence of an external magnetic field parallel to the junction barrier, Fiske steps occur in the IVC at finite voltages. In contrast to previous LTSEM experiments, we study the dynamic behavior of Josephson tunnel junctions (see also Ref. 20). In small junctions these dc-current steps in the IVC can be explained by the resonant excitation of the junction cavity modes,[21,22] where the corresponding ac current interacts with the ac-Josephson current. The cavity is formed by the junction electrodes and the insulating barrier.

For a rectangular two-dimensional junction with length L and width W the resonance voltage $V_{m;n}$ is given by[23]

$$V_{m;n}=\frac{h\bar{c}}{4e}\left[\left[\frac{m}{W}\right]^2+\left[\frac{n}{L}\right]^2\right]^{1/2}. \tag{1}$$

The integers m,n characterize the Fiske mode, h is Planck's constant, $\bar{c}$ the Swihart velocity,[24] and e the elementary charge.

For magnetic fields $\mathbf{H}=H_x\mathbf{e}_x$ ($\mathbf{H}=H_y\mathbf{e}_y$, respectively) parallel to the junction edge only one-dimensional cavity modes with corresponding voltages $V_{m;0}$ ($V_{0;n}$) are excited. Two-dimensional excitations are generated for arbi-

trary orientations of the magnetic field within the barrier plane.

With our measurement techniques we are able to confirm directly the theoretical assumption of cavity modes in a tunnel junction of intermediate size. In addition to one-dimensional modes clearly displayed in the LTSEM images, the two-dimensional excitations are also shown. Beyond the results presented in this paper, there is no basic difficulty to extend the developed model and measurement techniques to any junction geometry of interest as long as the junction is not large compared to the Josephson penetration depth λ_J.

This paper is divided into six sections. In Sec. II we describe the experimental configuration and in Sec. III we present a qualitative model to understand the different signals of the whole junction due to the local electron-beam irradiation. The experimental results are shown and discussed in Sec. IV. Furthermore, we discuss in Sec. V numerical simulations for the one-dimensional case within the perturbed sine-Gordon model as a starting point for the quantitative explanation of our observations. In Sec. VI we summarize our conclusions.

II. EXPERIMENTAL SETUP

The principle of the LTSEM experiments and the orientation of the sample are shown in Fig. 1. In our experiments the silicon substrate with the Josephson tunnel junction was mounted on a single-crystalline sapphire disk using high-thermal-conductivity glue. The special cryostage described in Ref. 25 allows us to scan the sample surface with the electron beam of a conventional SEM while the back side of the sapphire disk is in direct contact with liquid helium. A sufficiently homogeneous magnetic field parallel to the junction barrier is generated by two crossed pairs of superconducting coils inside the liquid helium tank of the cryostage. For values of the magnetic field up to 10 mT perpendicular to the electron beam we observed only a constant shift of the electron beam but no overall reduction of the LTSEM resolution.

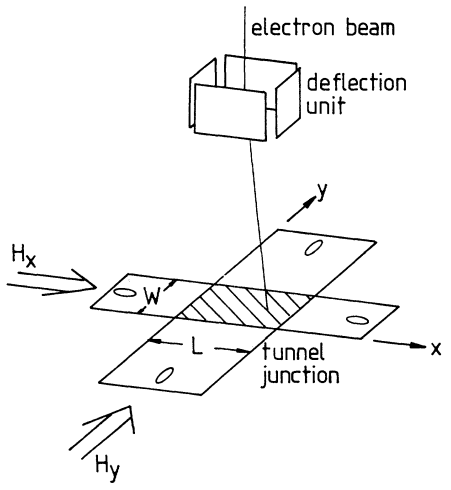

FIG. 1. Schematic principle of the LTSEM experiments and orientation of the tunnel junction.

In contrast to the usual SEM, the LTSEM resolution is given by the thermally disturbed area. The electron-beam irradiation of superconducting niobium or lead thin-film samples results in a local heating effect.[26,27] The thermally perturbed area is determined by the thermal healing length η

$$\eta=\left[\frac{\kappa D}{\alpha_{\rm th}}\right]^{1/2}, \tag{2}$$

where κ and D are the heat conductivity and the thickness of the irradiated film, respectively. The heat-transfer coefficient $\alpha_{\rm th}$ describes the thermal flux flowing from the thin film into the substrate. We note that for our experimental conditions (acceleration voltage 25 kV, beam current 10^{-12}–10^{-10} A) both electrodes of the junction are uniformly perturbed along the z direction and η is about three times larger than the best spatial resolution of the various imaging techniques. Typically the spatial resolution of LTSEM measurements on Josephson junctions is about 1 μm. In the voltage-imaging technique the junction is biased at a fixed current I_B for the Fiske step of interest. The value and direction of the external magnetic field are chosen to get the most stable conditions for the investigated state of the junction. In order to obtain a better signal-to-noise ratio, the electron beam is periodically modulated by a beam-blanking unit (20 kHz) and the corresponding voltage change $\Delta V_{m;n}$ (typically 10^{-8}–10^{-6} V) is detected phase sensitively by a lock-in amplifier. For the current images we detect the electron-beam-induced change of the maximum Fiske-step current $\Delta I^{\rm max}_{m;n}$. The corresponding magnetic field was chosen to get the maximum step height in the IVC. The experimental setup for the current images is described in detail in Ref. 12.

III. QUALITATIVE MODEL FOR THE LTSEM SIGNAL

In this section we present a qualitative model which explains the signal generation for the two imaging techniques without using numerical simulations. The model is based on the change of the junction quality factor due to the local electron beam heating.

We are looking at small rectangular Josephson tunnel junctions with length L and width W both smaller than $2\pi\lambda_J$, where λ_J is the Josephson penetration depth given by $\lambda_J=(\hbar/2ed\mu_0 j_1)^{1/2}$ (μ_0 is the permeability, $d=2\lambda_L+b$, λ_L is the London penetration depth, $\hbar=h/2\pi$, b is the barrier thickness, and j_1 is the average critical current density). Including the bias current density j we obtain the basic equation for the junction phase difference $\varphi(x,y,t)$ (Ref. 28)

$$\left[\beta\left[\frac{\partial^3}{\partial t\partial x^2}+\frac{\partial^3}{\partial t\partial y^2}\right]+\frac{\partial^2}{\partial x^2}+\frac{\partial^2}{\partial y^2}-\frac{\partial^2}{\partial t^2}-\alpha\frac{\partial}{\partial t}\right]\varphi(x,y,t)=f(x,y)\sin\varphi(x,y,t)+\gamma\ , \tag{3}$$

with the boundary conditions

$$\frac{\partial\varphi}{\partial x}(0,y)=\frac{\partial\varphi}{\partial x}(l,y)=k_y;$$
$$\frac{\partial\varphi}{\partial y}(x,0)=\frac{\partial\varphi}{\partial y}(x,w)=-k_x\ , \tag{4}$$

and with $k_x=H_x^{\rm ext}/(\lambda_J j_1)$ and $k_y=H_y^{\rm ext}/(\lambda_J j_1)$. Equations (3) and (4) are written in normalized units. The spatial coordinates are normalized to the Josephson penetration depth λ_J whereas the time is measured in units of the inverse plasma frequency ω_0^{-1}, which is given by $\omega_0=[2ej_1/(\hbar C_s)]^{1/2}$, where C_s is the capacitance per unit area, $l=L/\lambda_J$ and $w=W/\lambda_J$ denote the normalized length and width of the junction, respectively. $f(x,y)$ represents the spatial distribution of the normalized critical current and is equal to unity in a homogeneous junction. In the following we also use the magnetic field $\mathbf{h}=\mathbf{H}/(\lambda_J j_1)$ in normalized units and the bias current $\gamma=j/j_1$.

In Eq. (3) two loss terms are included. Surface losses due to the flow of normal conducting electrons within the superconducting electrodes are described in the β term on the left. We also take into account losses caused by the tunneling of normal conducting electrons (α term). Therefore the total quality factor is given by $Q^{-1}=Q_s^{-1}+Q_q^{-1}$ where Q_s^{-1} describes the surface losses and Q_q^{-1} the quasiparticle tunneling losses, respectively. We neglect contributions such as dielectric, radiation, or geometrical losses discussed in Ref. 29.

For solving Eq. (3) we neglect the influence of the bias current γ and use the following ansatz which fulfills the boundary conditions (4):

$$\varphi(x,y,t)=\omega t-k_x y+k_y x+\psi_{m;n}\ . \tag{5}$$

According to our experimental conditions where the junction is biased nearly at resonance we set the angular frequency $\omega\approx\omega_{m;n}$ and we assume that only one cavity mode of frequency $\omega_{m;n}$ with the wave vector $(k_n;k_m;0)=(n\pi/l;m\pi/w;0)$ is significantly excited. Therefore $\psi_{m;n}$ can be written as[28]

$$\psi_{m;n}(x,y,t)=a\cos(k_n x)\cos(k_m y)\sin(\omega_{m;n}t+\theta)\ . \tag{6}$$

This ansatz implies that the junction is acting like an open-ended cavity where the electric (magnetic) field caused by $\psi_{m;n}$ has antinodes (nodes) at the junction corners.

Next we discuss the influence of the local electron beam induced heating upon the Fiske mode. For simplicity we look at a normalized area of dimension $\epsilon^2=4\eta^2/\lambda_j^2$ and of square shape uniformly perturbed by the electron beam. The local temperature increase causes a local increase of the quasiparticle density in the perturbed area and therefore a change in both contributions Q_s, Q_q to the junction quality.

First, we deal with the change of Q_q due to the local irradiation. Following Ref. 29, Q_q is proportional to the total tunneling conductance σ_q of quasiparticles. σ_q increases by the amount $\Delta\sigma_q$ which is in general a function of the coordinates of the beam focus (x_0,y_0) and of the electron beam parameters (beam power, ϵ^2). Neglecting effects due to the finite size of the perturbed area at the junction boundaries, $\Delta\sigma_q$ is independent of the beam position across the junction surface if the tunneling conductivity is homogeneous. Therefore, the beam-induced change ΔQ_q is assumed to be independent of the beam position (x_0,y_0) on the junction.

Second we discuss the relation between Q_s and the beam position. Q_s is determined by the time-averaged energy stored in the cavity divided by the surface power losses P_s. Using classical electrodynamics P_s can be calculated to be[30]

$$P_s=\lambda_J^4 j_1^2\int_0^l\int_0^w dx\,dy\,R_s|\mathbf{n}\times\mathbf{h}^{\psi}(\mathbf{r})|^2\ , \tag{7}$$

where R_s is the real part of the surface impedance $Z_s=R_s+i\chi_s$, $\mathbf{h}^{\psi}(\mathbf{r})$ is the normalized time independent part of the magnetic field caused by $\psi_{m;n}$, and $\mathbf{n}$ is a unit vector perpendicular to the junction surface. At this point we have to mention that the temporal resolution of LTSEM is determined by thermal processes with relaxation times of typically 10^{-7} s (Ref. 26) and, therefore, is some orders of magnitude less than the period of the standing wave for our junctions (see also Sec. IV). In this sense we can use the time-averaged equation (7) and deal only with time-averaged signals in our model.

In the case of the extreme London limit we can approximate R_s to be

$$R_s\approx\tfrac{1}{2}(\omega\mu_0)^{1/2}\sigma_{s1}/\sigma_{s2}^{3/2} \tag{8}$$

with the surface conductivity $\sigma_s=\sigma_{s1}-i\sigma_{s2}$ and $\sigma_{s2}\gg\sigma_{s1}$ where the supercurrents dominate the normal currents.[31] Within the two-fluid model σ_{s1} is proportional to the density of the normal conducting electrons and the temperature dependence of $R_s(T)$ can be calculated phenomenologically[31]

$$R_s(T)=\frac{1}{2}\mu_0^2\lambda^3\omega^2\sigma_{sn}\frac{(T/T_C)^4}{[1-(T/T_C)^4]^{3/2}}\ , \tag{9}$$

where σ_{sn} denotes the surface conductivity just above the transition temperature T_C of the junction electrodes and λ is the ac-magnetic penetration depth at zero temperature.

A temperature increase ΔT in the irradiated area causes an increase ΔR_s of R_s and therefore a change of the total surface losses ΔP_s of the junction cavity

$$\Delta P_s(x_0,y_0)=\lambda_J^4 j_1^2\int_{x_0-\epsilon/2}^{x_0+\epsilon/2}\int_{y_0-\epsilon/2}^{y_0+\epsilon/2}dx\,dy\,\Delta R_S[(h_x^{\psi}(x,y))^2+(h_y^{\psi}(x,y))^2] \tag{10}$$

$$\approx(a\epsilon j_1\lambda_J^2)^2\Delta R_S[k_n^2\sin^2(k_n x_0)\cos^2(k_m y_0)+k_m^2\cos^2(k_n x_0)\sin^2(k_m y_0)]\ . \tag{11}$$

For this we used Eq. (6) and $\nabla\psi=\mathbf{h}^{\psi}\times\mathbf{e}_z$ to calculate the magnetic field $\mathbf{h}^{\psi}(\mathbf{r})$. We obtained Eq. (11) with the approximation $k_n\epsilon$ and $k_m\epsilon\ll 1$ supposing that the irradiated area is small compared to the wavelength of the standing wave. The time-averaged energy stored in the cavity is determined by the surface inductance χ_s depending on σ_{s2}. Therefore this energy is nearly temperature independent.[32]

Combining both loss mechanisms in the case of weak electron-beam perturbation the change of the junction Q is expected to be

$$\Delta Q\approx c_1+c_2(k_n^2\sin^2(k_n x_0)\cos^2(k_m y_0)+k_m^2\cos^2(k_n x_0)\sin^2(k_m y_0))\ . \qquad (12)$$

The constants c_1 and c_2 correspond to ΔQ_q (independent) and ΔQ_s (dependent on the beam position), respectively.

For obtaining voltage images of a Fiske mode, the tunnel junction is current biased on a given Fiske step $(m;n)$ at voltage $V_{m;n}$. Irradiating the junction with the electron beam results in a beam-induced voltage shift $\Delta V_{m;n}$.

First, for simplicity we assume a linear relationship between ΔQ and the detected voltage change $\Delta V_{m;n}$. This assumption is based on the model for low-Q junctions developed by Kulik,[21] where the IVC's have Lorentzian shape near the resonance voltage. A decrease of the quality factor causes first a broadening and second a shift of the Lorentzian shape to lower voltages. Corresponding to our experimental conditions where less than 3% of the whole junction area are effectively perturbed by the electron beam, this linear behavior appears well justified. Therefore, using the voltage-imaging technique the detected signals ΔV should satisfy Eq. (12).

For the current-imaging technique the electron beam induced change of the maximum Fiske-step current $\Delta I_{m;n}^{\max}$ is detected. The relation between the signal $\Delta I_{m;n}^{\max}$ and the change of the junction quality Q can be explained for the one-dimensional case by the function $I_{m;0}^{\max}(Q), I_{0;n}^{\max}(Q)$, respectively. The general shape of this function is described in Refs. 33 and 34. The sign of $\Delta I_{m;n}^{\max}$ depends on the value of the quality factor for the investigated state. For values of Q higher (lower) than $Q_{\max}$, which corresponds to the maximum step height, the electron beam induced decrease of Q can cause an increase (decrease) of $I_{m;n}^{\max}$. The maximum relative change $|\Delta I_{m;n}^{\max}/I_{m;n}^{\max}|$ in our experiments was less than 5%. Therefore we also expect $\Delta I_{m;n}^{\max}\propto|\Delta Q|$ due to the weak influence of the electron beam. So, at least for the one-dimensional case the shape of the expected signals in the current-technique is also given by Eq. (12). However the sign of $\Delta I_{m;n}^{\max}$ can change from one state to the other.

IV. EXPERIMENTAL RESULTS

The $Nb/Al_2O_3/Nb$ tunnel junctions have been fabricated at the Electrotechnical Laboratory (Tsukuba, Japan). A detailed description of the fabrication process together with more information about the geometry can be found in Ref. 35. We checked the homogeneity of the junction using LTSEM and observing the distribution of the energy gap and the tunneling conductivity. In all cases no relative inhomogeneity larger than 5% was observed over the whole tunneling area of $50\times 50\ \mu m^2$ within the spatial resolution of the LTSEM (3 μm). The critical current density was $j_1=245\ A/cm^2$. By means of the Fraunhofer diffraction pattern we determined the London penetration depth of the Nb-electrodes as $\lambda_L=88$ nm and the Josephson penetration depth as $\lambda_J=24.4\ \mu m$. So the junction is of intermediate size ($L/\lambda_J=W/\lambda_J=2.0$). As we expected from the nearly symmetrical Fraunhofer diffraction pattern, we observed only a slight deviation from a homogeneous Josephson current distribution in the LTSEM images due to self-field effects. All experiments were carried out in the LTSEM metal cryostage at a bath temperature of 2.8 K.

A. One-dimensional modes

For each direction of the magnetic field parallel to one junction edge, e.g., $\mathbf{H}=H_y\mathbf{e}_y$, all steps up to the eighth were clearly visible in the IVC displayed on an oscilloscope. We obtained a slight difference of about 5% between the resonance voltages for the different field orientations, e.g., $V_{1;0}=200\ \mu V$ and $V_{0;1}=210\ \mu V$, which can be explained by the geometry of the wiring connecting the Nb top electrode. Using $V_{0;1}$ we determined the capacitance per unit area $C_s=4.3\ \mu F/cm^2$ and $\bar{c}/c=0.033$. This corresponds to a frequency of the standing wave of 99.1 GHz. Figure 2 shows voltage images of the Fiske modes $n=1-6$. The magnetic field is oriented in the $\mathbf{e}_y$ direction and therefore perpendicular to the scan direction of the electron beam. The corresponding experimental parameters are listed in Table I. The deviation of the measured $V_{0;n}$ from the values $nV_{0;1}$ in Table I reflects the frequency dependence of λ_L.[32]

The basic results of the voltage images of the one-dimensional Fiske modes are the following.

(1) $\Delta V_{m;n}$ is always negative for the used values of the bias current I_B.

TABLE I. Experimental parameters for the voltage images shown in Fig. 2 for the different Fiske steps.

Step order n		1	2	3	4	5	6
Resonant voltage $V_{0;n}$	μV	210	410	605	795	960	1140
Magnetic field k_y	$\lambda_j j_1$	2.8	−4.4	5.3	7.2	8.5	10.5
Maximum step current	mA	1.0	1.3	1.5	1.1	0.8	0.7
Bias current I_B	mA	0.6	0.6	1.0	0.6	0.6	0.6

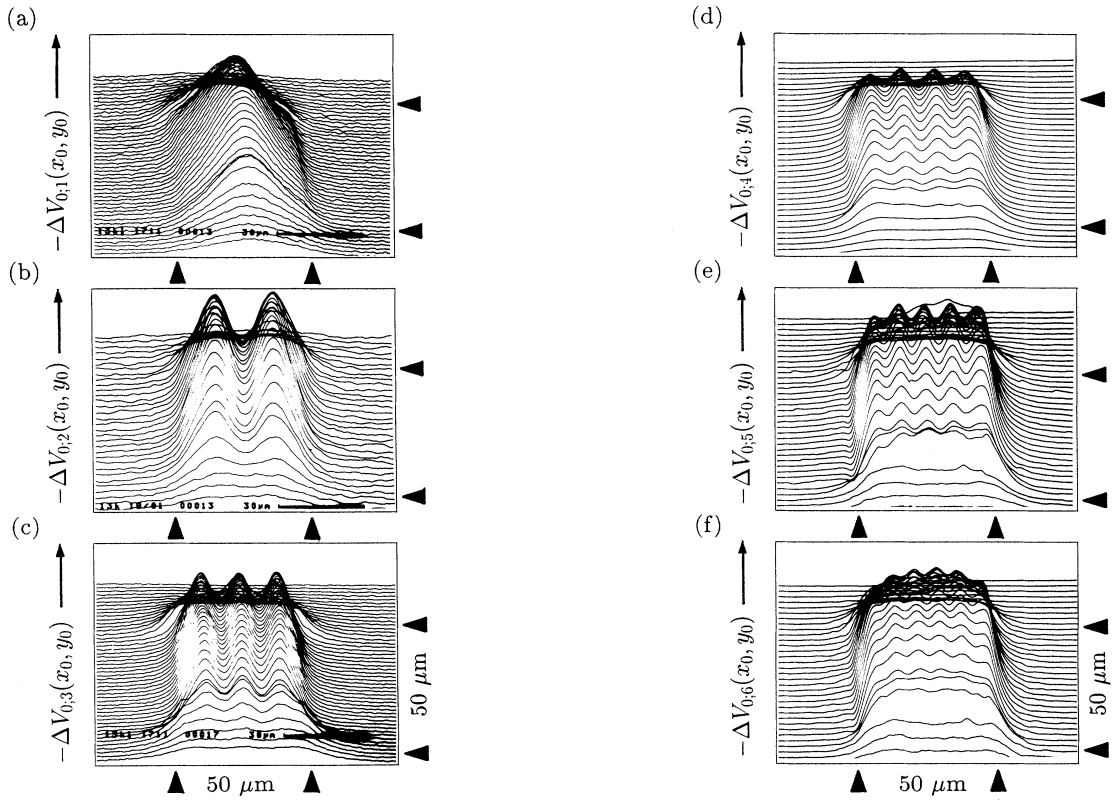

FIG. 2. Y-modulation voltage images of the Fiske modes $(0;n)$ with $n=1-6$. For all images the magnetic field is parallel to $\mathbf{e}_y$. (a)–(f) correspond to $n=1-6$. The experimental parameters are listed in Table I. The arrows mark the junction boundaries.

(2) A change in the sign of I_B results in a change in sign of $\Delta V_{m;n}$.

(3) The modulation of the detected signal is always perpendicular to the applied magnetic field and axially symmetrical to the middle of the junction. Taking images with applied fields parallel to the scan direction, the voltage change $\Delta V_{m;n}$ is constant over the whole tunneling area along each line scan.

(4) For different current feedings to the junction of nearly cross-type geometry the LTSEM images did not change significantly. Also no qualitative change is seen, if the magnetic field direction is reversed. This behavior is expected in the model for junctions of this size.

All our basic results follow directly from the Q-factor model described in Sec. III. Analyzing the experimental data of Fig. 2 we obtain also some semiquantitative results. For increasing the bias current I_B on a step the maximum amplitude of ΔV decreases. This effect is a direct consequence of the imaging technique and not correlated to the fundamental physics where for increasing I_B an increase of the amplitude of the standing wave excitation a is expected. The decreasing stability of the Fiske state with increasing step current determined the values of the possible bias currents I_B in our experiment. In most cases it was not possible to chose I_B higher than about half the maximum step current.

Furthermore, holding the beam parameters and I_B constant, the maximum electron-beam induced signal ΔV increases with the step order, e.g., from 150 nV for the first up to 1.5 μV for the sixth step at a fixed value $I_B=0.5$ mA.

Figure 3 shows the comparison between our model and the experimental results. For this we recorded a single line scan across the middle of the junction and plotted $-\Delta V_{0;n}(x_0, W/2)$. In contrast to Eq. (12) now we take into account the nonvanishing diameter of the area perturbed by the electron beam. The calculation was done for a one-dimensional geometry of a single line scan. The finite spatial resolution of the imaging technique was taken into account by a constant temperature rise across the length ϵ. We estimate ϵ to be 0.32 and integrate Eq. (10) analytically. For fitting the calculated line scans to the experimental data we determined the constants c_1 and c_2. Presumably, the difference between the calculated curves and the experimental data, especially at the junction boundaries can be explained by a more realistic temperature profile. In addition, the spatial extension of the perturbed area perpendicular to the scan direction has to be taken into account.

Using the current imaging technique, in principle we obtained the same results. In Fig. 4 the third and fourth steps are shown. With this method we were able to display even the seventh Fiske step. Hence, we conclude that the spatial resolution is definitely better than 3 μm.

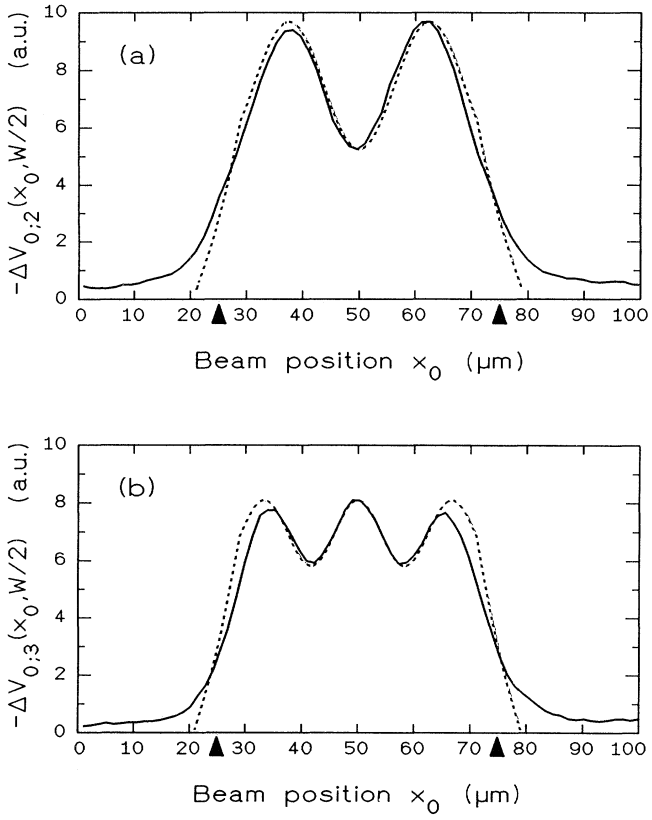

FIG. 3. Comparison of the experimental data (solid lines) and the calculated signal (dashed lines) using the Q-factor model for (a) the (0;2) and (b) the (0;3) modes. The arrows mark the junction edges.

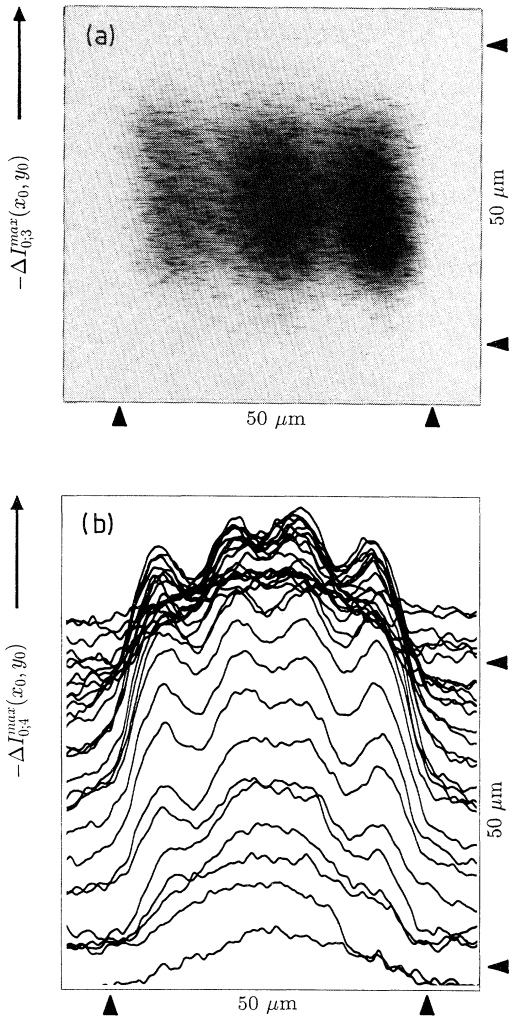

FIG. 4. One-dimensional Fiske modes in the current-imaging technique. The magnetic field is parallel to $\mathbf{e}_y$. (a) Brightness modulation image of the third Fiske mode with $I^{max}_{0;3} = 1.5$ mA. (b) Y-modulation picture for the fourth step with $I^{max}_{0;4} = 1.0$ mA. For both images the maximum relative depression $|\Delta I^{max}_{0;n}/I^{max}_{0;n}|$ due to the electron beam irradiation is less than 5%.

We could not observe steps higher in order than $n = 7$, because those steps were unstable during the irradiation.

Only for the first and second steps the irradiation of the junction results in an increase of the maximum step height. This behavior is expected from the approximation of Q for the different steps together with the fundamental function $I^{max}_{0;n}(Q)$ of Ref. 33 which passes through its maximum if we change from the second to the third step. From all these results we see that our model provides a good qualitative understanding of the observed signals.

B. Two-dimensional modes

We have obtained cavity mode excitation for magnetic fields oriented nearly diagonally across the junction barrier. In this case two-dimensional cavity modes are excited. We have observed steps in the IVC corresponding to the modes $(n;m) = (1;1)$, (1;2) or (2;1), (2;3) or (3;2), and (3;3). Figure 5(a) shows the (1;1) mode in the voltage imaging technique whereas the signal calculated from our model is displayed in Fig. 5(b). The excitation of two-dimensional modes is clearly observed in qualitative agreement with the calculation. Using LTSEM one is able to distinguish between, e.g., the (2;1) and (1;2) mode directly which is not possible for a square junction by means of the IVC alone.

V. NUMERICAL SIMULATIONS: THE CHANGE OF THE CRITICAL CURRENT DENSITY

In order to provide some qualitative support we performed the numerical simulations in explaining our experiments. In this section we study the signal generation model which is to some extent alternative to those one described in the previous section. Let us suppose, that the only factor which is responsible for the electron beam induced change of the IVC of the Josephson junction is the local variation of the superconducting critical current density j_1. Due to the local heating of the junction elec-

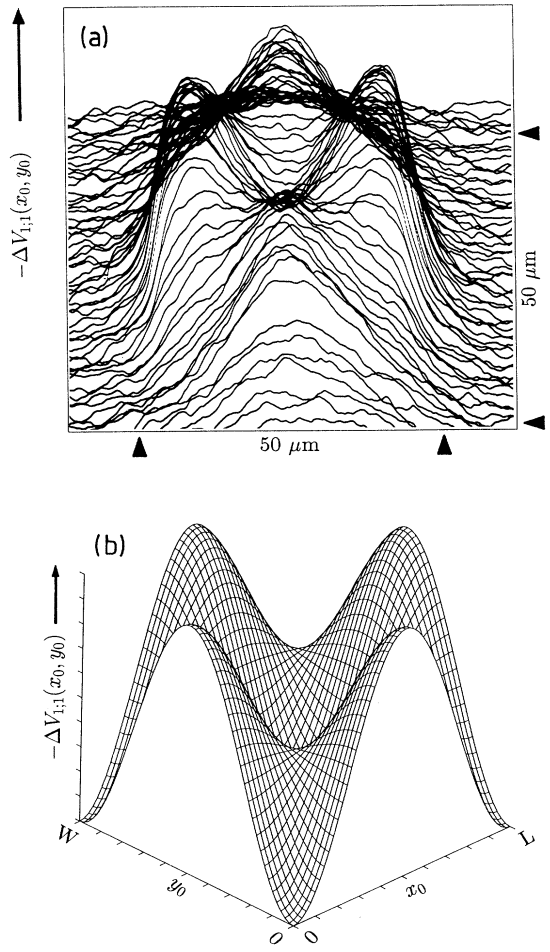

FIG. 5. (a) Y-modulation voltage image of the two-dimensional (1;1) mode with $V_{1;1}=310\ \mu$V. The magnetic field is oriented nearly diagonally from the lower left to the upper right corner of the junction. (b) Calculated signal for the (1;1) mode using Eq. (12). For better visibility the junction is rotated about 45° relative to (a) and only the spatially modulated part of the signal is shown.

trodes produced by the electron beam, the j_1 value must be suppressed in this area. We use a quasi-one-dimensional version of Eq. (3) with φ depending only on the spatial coordinate x. This approximation is good enough for the case $H_x^{\text{ext}}=0$. For the sake of simplicity we use the explicit numerical algorithm[36] and do not take the β dissipative term into account. In the experiment the area of the junction which is irradiated by the electron beam may be considered as a local "microresistor." In numerical calculations we approximate such an inhomogeneity by the function[36]

$$f(x)=1-\epsilon\left[1-\tanh^2\frac{2(x-x_0)}{\epsilon}\right], \tag{13}$$

where x_0 is the position of the electron beam in the junction, $\epsilon>0$. Equation (3) was solved numerically with the boundary conditions (4) and $k_x=0$.

We studied the junction with the normalized junction length $l=2.0$ and the dissipation coefficient $\alpha=0.1$. In the numerical data presented below the averaged dimensionless voltage $u\sim(\partial\varphi/\partial\tau)$ is given in normalized units which are usually used in fluxon-dynamics calculations. The voltage of the first Fiske step is corresponding in these units to $u=0.5$. The details about the initial conditions and numerical algorithm of IVC calculations may be found elsewhere.[37] Figure 6 shows the numerically calculated IVC of the homogeneous junction with $f(x)\equiv 1$ at the magnetic field $k_y=3.7$. This value of the magnetic field has been chosen according to the typical experimental conditions during our measurements. In Fig. 6 one can clearly see a set of Fiske steps up to $n=3$.

In order to study numerically the influence of the electron beam on the voltage of the particular Fiske step (i.e., to simulate the voltage-imaging technique), we have calculated the change of the voltage of the step at a certain bias current value as a function of the inhomogeneity position x_0. The "strength" of the inhomogeneity we used was determined by $\epsilon=0.5$, which corresponds to a reasonable size of the Josephson junction area influenced by the electron beam in our experiment.

Figure 7 shows a typical profile of $f(x)$ we used in numerical simulations according to the formula (13) for the inhomogeneity placed inside the junction at the point $x_0=1.4$.

The numerically calculated voltage images we obtained for the first three Fiske steps are presented in Fig. 8. The negative change of the voltage of each step $-\Delta u$ is given in percents relative to the undisturbed voltage value u without the inhomogeneity in the junction. The inhomogeneity (13) was placed in the area outside the Josephson junction at $x_0=-1.0$ and then scanned across the whole junction to $x_0=3.0$.

The first feature which is common for all of the steps shown in Fig. 8 is that the average voltage u is increasing when the inhomogeneity is placed inside the Josephson junction ($-\Delta u<0$, i.e., $\Delta u>0$). In contrary, in the real

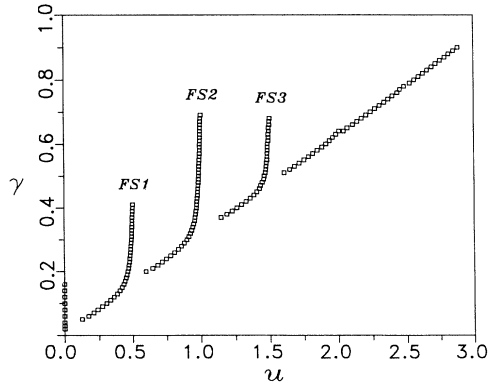

FIG. 6. Numerically calculated IVC of the Josephson junction without the local inhomogeneity [i.e., $f(x)\equiv 1$] in the magnetic field $k_y=3.7$ (other parameters are in text).

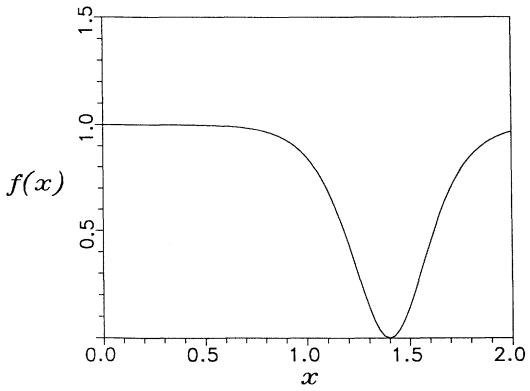

FIG. 7. The profile of the normalized superconducting critical current density $f(x)$ used in numerical simulations for the inhomogeneity placed in the junction at $x=x_0=1.4$.

physical experiment the voltage of the steps is decreasing and $\Delta V<0$. Here, it is important to emphasize that in this section we consider a kind of alternative model for the signal generation to those described in Sec. III, which is not including any change of dissipation in the Josephson junction when the electron beam is placed inside it. In fact, the local heating produced by the electron beam is always increasing the real part of the impedance of the Josephson junction and gives rise to the broadening of the Lorentzian-shape resonance (see Sec. III), i.e., to the decreasing of the step voltage. The model we consider here is taking into account only the local variation of the critical current density in the junction, which may influence the shape of the standing electromagnetic wave of the Fiske resonance.[38] So, for the comparison of the numerically simulated voltage images with the experiment one should look at the *spatial dependence* of the voltage response as long as the inhomogeneity is inside the Josephson junction, assuming that the spatially independent voltage decrease observed in the experiment is due to the dissipation which is not included in the present numerical model.

Comparing the curves in Figs. 8(a)–8(c) one can see the different number of maxima inside the junction, depending on the number of the Fiske step. This behavior shown by numerical simulations is in good agreement with the experimental results presented in Sec. IV. The number of the signal maxima is equal to the number of the Fiske step n. The relative amplitude of the spatially dependent voltage variation is about few percent, which is also in agreement with the experiment. The increase of the signal near the junction boundaries seen in the numerical simulations is due to the fact that the spatially independent step voltage response is negative and the step voltage increases when the beam is taken away from the junction. The noiselike oscillations seen in Fig. 8(c) are the artifact of the numerical voltage averaging algorithm.

A small asymmetry of Δu with respect to the middle of the junction is a nonlinear effect of the junction of the intermediate length ($l=2.0$) and it reverses with the reversing of the field k_y or the current γ. This asymmetry is

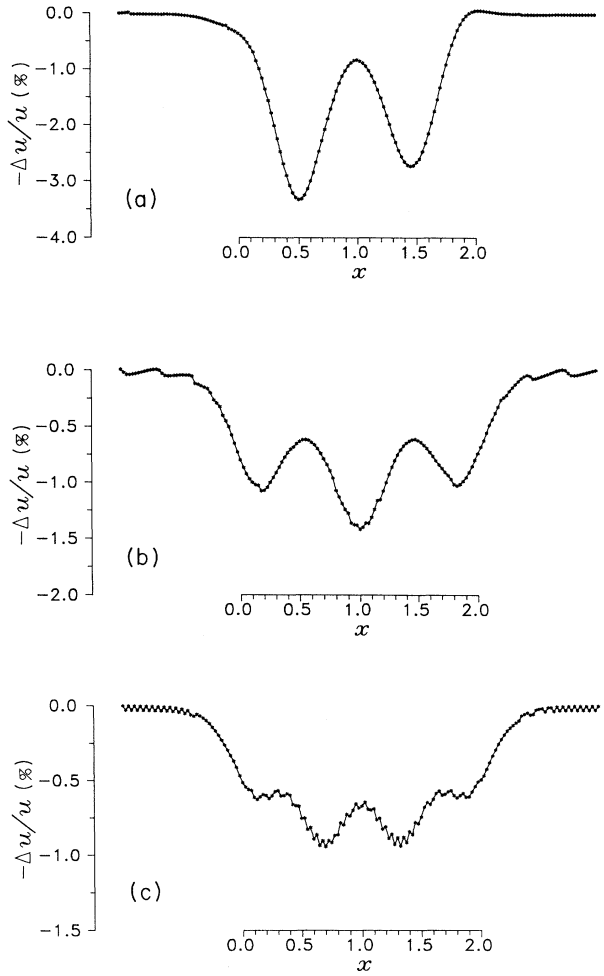

FIG. 8. The change of the averaged voltage $-\Delta u$ of the junction biased at the different Fiske steps (FS) as a function of the position of the inhomogeneity x_0: (a) FS1, $\gamma=0.25$; (b) FS2, $\gamma=0.50$; (c) FS3, $\gamma=0.50$.

rather small and has not been seen in the real experiment. We have also checked the field-value dependence of the $-\Delta u/u$ curves and found it not to be very sensitive.

In summary, in this section we have investigated a numerical model for the signal generation taking into account *only* the spatial variation of the critical current density due to the electron beam irradiation. The spatially dependent response of the Fiske step voltages we observed is in agreement with the experimental results. Hence, the simple dissipative mechanism of the signal generation in our experiment is not the only one, which should be taken into account in order to build the *quantitative* model for the voltage images of the Fiske steps produced by the electron beam scanning technique.

VI. CONCLUSIONS

We have used low-temperature scanning electron microscopy (LTSEM) to investigate dynamic states of Josephson tunnel junctions in an external magnetic field.

LTSEM is a powerful tool to obtain spatially resolved information about the complex behavior of a tunnel junction biased at a Fiske step. The electron beam power was reduced so far that the electron beam acts like a passive probe without destroying the dynamic state of the nonlinear system. The achieved spatial resolution is about 3 μm or better. A two-dimensional $Nb/Al_2O_3/Nb$ tunnel junction (50×50 μm^2) shows clearly one- or two-dimensional mode excitations depending on the orientation of the external magnetic field. We observed only one-dimensional Fiske modes if the magnetic field was parallel to one edge of the junction. Two-dimensional modes were observed for diagonal field orientation. For a square tunnel junction of intermediate size (relative length and width $L/\lambda_J = W/\lambda_J = 2.0$) the excitation of the junction cavity modes is clearly visible. Hence, the physical origin of the investigated Fiske steps in the IVC is the interaction between the ac-Josephson current and the standing waves formed by the junction cavity. For the interpretation of the LTSEM signal we have developed a qualitative model based on the beam-induced change of the quality factor of the junction resonator. Furthermore, we performed numerical simulations based on the perturbed sine-Gordon equation. For this we included only the local suppression of the critical current density. In order to describe properly the voltage images and the current images observed in the experiment, one should take into account both the dissipation and the critical current density perturbation generated by the electron beam in the Josephson junction. The spatially resolved measurements together with our models for the signal generation confirm earlier theoretical work on Josephson tunnel junctions of intermediate size, dealing with cavity mode excitations for the one-dimensional and the two-dimensional case.

ACKNOWLEDGMENTS

Financial support of this work by the Deutsche Forschungsgemeinschaft is gratefully acknowledged. The authors would like to thank R. Gross and M. Koyanagi, ETL, Ibaraki, Japan for manufacturing the square tunnel junction of high quality factor. One of the authors (A.V.U.) wants to thank the Alexander von Humboldt-Stiftung for financial support.

[1]R. P. Huebener, in *Advances in Electronics and Electron Physics,* edited by P. W. Hawkes (Academic, New York, 1988), Vol. 70, p. 1.

[2]E. Held, W. Klein, and R. P. Huebener, Z. Phys. B **75**, 223 (1989).

[3]R. P. Huebener, E. Held, and W. Klein, Mater. Sci. Eng. B **5**, 157 (1990).

[4]K. M. Mayer, R. Gross, J. Parisi, J. Peinke, and R. P. Huebener, Solid State Commun. **63**, 55 (1987).

[5]K. M. Mayer, J. Parisi, J. Peinke, and R. P. Huebener, Physica D **22**, 306 (1988).

[6]R. Gross, T. Doderer, R. P. Huebener, F. Kober, D. Koelle, C. Kruelle, J. Mannhart, B. Mayer, D. Quenter, and A. Ustinov, Physica B **169**, 415 (1991).

[7]R. Gross, J. Bosch, R. P. Huebener, C. C. Tsuei M. Scheuermann, M. M. Oprysko, and C. C. Chi, Nature (London) **332**, 818 (1988).

[8]D. Koelle, F. Kober, M. Hartmann, R. Gross, R. P. Huebener, B. Roas, L. Schultz, and G. Saemann-Ischenko, Physica C **167**, 79 (1989).

[9]P. W. Epperlein, H. Seifert, and R. P. Huebener, Phys. Lett. **92A**, 146 (1982).

[10]R. Gross, M. Koyanagi, H. Seifert, and R. P. Huebener, Phys. Lett. **109A**, 298 (1985).

[11]J. Bosch, R. Gross, M. Koyanagi, and R. P. Huebener, Phys. Rev. Lett. **54**, 1448 (1985).

[12]J. Bosch, R. Gross, M. Koyanagi, and R. P. Huebener, J. Low Temp. Phys. **68**, 245 (1987).

[13]J. Mannhart, J. Bosch, R. Gross, and R. P. Huebener, J. Low Temp. Phys. **70**, 459 (1988).

[14]J. Mannhart, J. Bosch, R. Gross, and R. P. Huebener, Phys. Rev. B **35**, 5267 (1987).

[15]J. Mannhart, J. Bosch, R. Gross, and R. P. Huebener, Phys. Lett. A **122**, 439 (1987).

[16]S. C. Meepagala, W. D. Shen, P. K. Kuo, and J. T. Chen, in *Low Temperature Physics,* Vol. **17**, edited by U. Eckern, A. Schmid, W. Weber, and H. Wühl (Elsevier-Science, North-Holland, Amsterdam, 1984), p. 473.

[17]S. Meepagala, J. T. Chen, and Jhy-Jiun Chang, Phys. Rev. B **36**, 809 (1987).

[18]M. D. Fiske, Rev. Mod. Phys. **36**, 221 (1964).

[19]D. D. Coon and M. D. Fiske, Phys. Rev. A **123**, 774 (1965).

[20]T. Doderer, D. Quenter, B. Mayer, C. A. Krulle, A. V. Ustinov, R. P. Huebener, J. Niemeyer, R. Fromknecht, R. Poepel, U. Klein, P. Dammschneider, and J. H. Hinken, in *Nonlinear Superconductive Electronics and Josephson Devices,* edited by N. F. Pedersen, M. Russo, A. Davidson, C. Costabile, and S. Pagano (Plenum, New York, to be published).

[21]I. O. Kulik, Pis'ma Zh. Eksp. Teor. Fiz. **2**, 134 (1965) [JETP Lett. **2**, 84 (1965)].

[22]R. E. Eck, D. J. Scalapino, and B. N. Taylor, Phys. Rev. Lett. **13**, 15 (1964).

[23]M.A.H. Nerenberg, P. A. Forsyth, Jr., and J. A. Blackburn, J. Appl. Phys. **47**, 4148 (1976).

[24]J. C. Swihart, J. Appl. Phys. **32**, 461 (1961).

[25]T. Doderer, H.-G. Wener, R. Moeck, C. Becker, and R. P. Huebener, Cryogenices **30**, 65 (1990).

[26]J. R. Clem and R. P. Huebener, J. Appl. Phys. **51**, 2764 (1980).

[27]R. Gross and M. Koyanagi, J. Low. Temp. Phys. **60**, 277 (1985).

[28]H. Svensmark, in *SQUID'85,* edited by H. D. Hahlbohm and H. Lübbig (Walter De Gruyter, Berlin, 1985), p. 471.

[29]T. C. Wang and R. J. Gayley, Phys. Rev. B **18**, 293 (1978).

[30]J. D. Jackson, *Classical Electrodynamics* (Wiley, New York, 1975), Chap. 8.

[31]J. H. Hinken, *Supraleiter-Elektronik* (Springer, Berlin, 1988).

[32]R. F. Broom and P. Wolf, Phys. Rev. B **16**, 3100 (1977).

[33]G. Paternò and J. Nordman, J. Appl. Phys. **49**, 2456 (1978).

[34]A. Barone and G. Paternò, *Physics and Applications of the Josephson Effect* (Wiley, New York, 1982).

[35]F. Hebrank, S. Lemke, R. P. Huebener, and R. Gross, Nucl. Instrum. Methods **A288**, 541 (1990).
[36]A. A. Golubov and A. V. Ustinov, IEEE Trans. Magn. **23**, 781 (1987).
[37]A. V. Ustinov, Phys. Lett. **136**, 155 (1989).
[38]If the Josephson junction is long enough and the Fiske step is corresponding to the soliton mode resonance, then the tendency of the step voltage to increase while the inhomogeneity is placed inside the junction is easy to understand. A local area of the decreased critical current density ("microresistor") attracts a soliton, thereby increasing the frequency of soliton oscillations and hence, the step voltage.

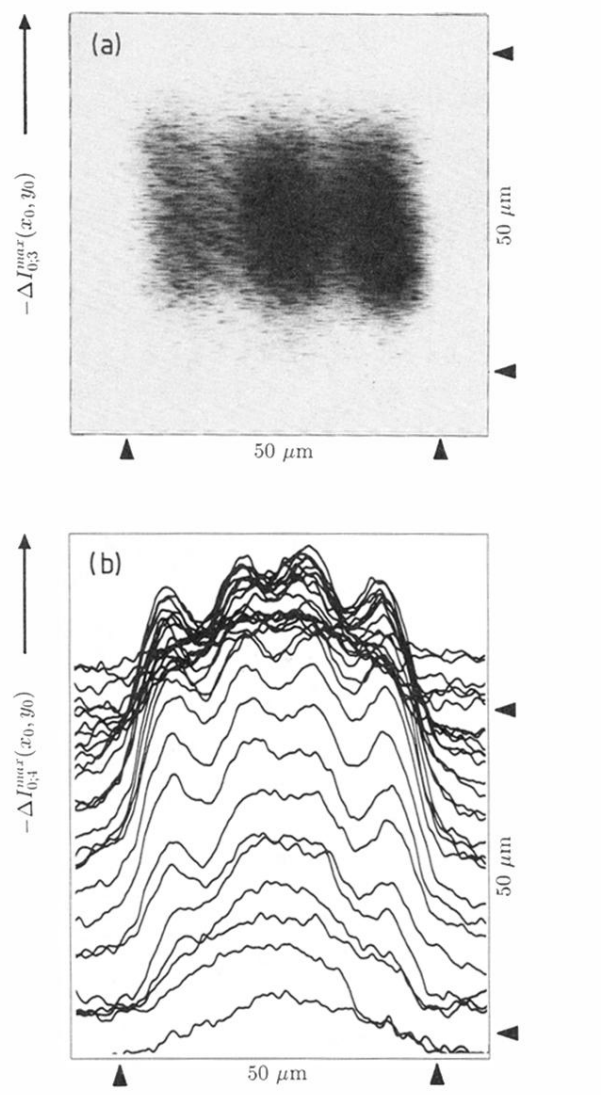

FIG. 4. One-dimensional Fiske modes in the current-imaging technique. The magnetic field is parallel to $\mathbf{e}_y$. (a) Brightness modulation image of the third Fiske mode with $I_{0;3}^{\max} = 1.5$ mA. (b) Y-modulation picture for the fourth step with $I_{0;4}^{\max} = 1.0$ mA. For both images the maximum relative depression $|\Delta I_{0;n}^{\max}/I_{0;n}^{\max}|$ due to the electron beam irradiation is less than 5%.